Supporting information for one bicopper complex with good affinity to nitrate for highly selective electrocatalytic nitrate reduction to ammonia

Kang-Yu Zeng [1], Jun-Jie Wang [2,*], Xiang Fang[2], Zuo-Xi Li [1,*]

[1] Institute of Materials Science and Devices, School of Material Science and Engineering, Suzhou University of Science and Technology, Suzhou 215009, China
[2] School of Chemistry and Chemical Engineering, and Anyang Key Laboratory of New Functional Complex Materials, Anyang Normal University, Anyang 455000, China
* Correspondence: lizx@usts.edu.cn (J.-J.W.), jjwang@aynu.edu.cn (Z.-X.L.)

ECSA evaluation

With regard to the ECSA evaluation, the electrochemical double-layer capacitance method was employed. All electrodes were reduced at −0.63 V vs. RHE for 2 min, and scanned in 1 M KOH at the sweep rate of 20, 40, 60, 80, and 100 mV s^{-1}. Ar was purged during the measurement. The potential range was 0.3 to 0.34 V vs. RHE for the Ce-doped Cu electrodes. The differences in these two current densities (Δj) at different sweep rates were then calculated and plotted against the sweep rates for each catalyst. By conducting linear fitting, we calculated the slopes of the Δj vs. sweep rate curves, which are the double-layer capacitances for different catalysts[29,30].

Ion-concentration detection methods

The pre-test and post-test electrolytes were obtained from the electrolytic cell, diluted, and adjusted to a neutral pH with concentrated sulfuric acid, and then determined with UV-Vis spectrophotometry (UV-2600i). The concentrations of nitrate-N, nitrite-N, and ammonia-N were measured by UV-Vis spectrophotometry according to the standard methods. The specific approaches are as follows[3].

Determination of nitrate-N

A total of 100 μL 1 M HCl and 10 μL 0.8 wt% sulfamic acid solution were added to the above 5 mL diluted solution. The absorption spectra were measured by

UV-Vis spectrophotometry and the absorption intensities at wavelengths of 220 and 275 nm were recorded. The final absorbance value was calculated by: $A = A_{220nm} - 2A_{275nm}$. The concentration–absorbance curves were plotted with a series of standard potassium nitrate solutions.

Determination of nitrite-N

A mixture of ρ-aminobenzenesulfonamide (4 g), N-(1-Naphthyl) ethylenediamine dihydrochloride (0.2 g), ultrapure water (50 mL), and phosphoric acid (10 mL, ρ = 1.70 g/mL) was used as a chromogenic reagent. Next, 100 μL of mixed color reagent was added to the above 5 mL diluted solution and mixed evenly, and the absorption intensity at a wavelength of 540 nm was recorded after standing for 20 min. The concentration–absorbance curves were calibrated using a series of standard sodium nitrite solutions.

Determination of ammonia-N

Potassium sodium tartrate solution (ρ = 500 g/L) was added to the above 5 mL diluted solution and mixed evenly, and then 0.1 mL Nessler's reagent was added to the solution. After standing for 20 min, we recorded the absorption intensity at a wavelength of 420 nm. The concentration–absorbance curves were calibrated using a series of standard ammonium chloride solutions.

Calculation of the yield, selectivity, and Faradaic efficiency

With regard to nitrate electroreduction, the NH_3 yield rate was calculated by Eq. 1:

$$NH_3 \text{ yield rate} = (c_{NH_3} \times V) / (M_{NH_3} \times t \times S) \quad (1)$$

The conversion rate can be calculated as follows:

$$NO_3^- \text{ Conversion} = \Delta c_{NO_3^-} / c_0 \times 100\% \quad (2)$$

The selectivity of ammonia was obtained by Eq. 3:

$$NH_3 \text{ Selectivity} = c_{NH_3} / \Delta c_{NO_3^-} \times 100\% \quad (3)$$

The Faradaic efficiency was defined from the electric charge consumed for synthesizing ammonia and the total charge passed in the electrode, according to Eq. 4:

$$\text{Faradaic efficiency} = (8F \times c_{NH_3} \times V)/(M_{NH_3} \times Q) \quad (4)$$

where c_{NH_3} is the mass concentration of NH_3-N (aq), V is the volume of electrolyte in the cathode compartment (40 mL), M_{NH_3} is the molar mass of NH_3-N, t is the electrolysis time (5 h), S is the geometric area of working electrode (1 cm^2), $\Delta c_{NO_3^-}$ is the concentration difference of NO_3^- before and after electrolysis, c_0 is the initial concentration of NO_3^-, F is the Faradaic constant (96485 C mol^{-1}), and Q is the total charge passed in the electrode[5].

Ion chromatography

Considering the influence of the hydroxylamine, the concentrations of ammonium, nitrite, and nitrate were further quantified by ion chromatography for comparison with colorimetric methods. The ion chromatography measurements were carried out on the Shine CIC-D100. The calibration curve of ammonium was created as follows: First, a series of NH_4Cl solutions with known concentrations (0.02, 0.04, 0.06, 0.08, 0.1 ppm) were prepared as standards. Next, standard curves of ion chromatography were calibrated using a series of standard NH_4Cl solutions. Finally, the post-test electrolyte was diluted to the standard curve range and injected into the ion chromatograph. The results were introduced into the template to calculate its concentration. The standard curves for nitrate and nitrite were created in the same way as above-mentioned, with the exception that NH_4Cl was replaced with $NaNO_3$ and $NaNO_2$, respectively.

X-ray single-crystal diffraction data of complex 1

X-ray single-crystal diffraction data of complex 1 were collected on a Rigaku MM-007/Saturn 70 with graphite monochromatic Mo-Kα radiation (= 0.71073 Å). The program SAINT (Bruker AXS, SAINT Software Reference Manual, Madison, WI, 1998.) was used for integration of the diffraction profiles. The structure was solved by direct method using the SHELXS program of the SHELXTL package and refined by full-matrix least-squares methods with SHELXL (SHELDRICK G.

SHELXTL NT, Program for solution and refinement of crystal structures, version 5.1. University of Göttingen: Göttingen, Germany, 1997.). The copper atom was located from the E-maps and other non-hydrogen atoms were located in successive difference Fourier syntheses, which are refined with anisotropic thermal parameters on F2. Hydrogen atoms of organic ligand were generated theoretically onto specific atoms and refined isotropically. However, the hydrogen atoms of water molecule were added by difference Fourier maps, and refined using a riding model. Crystallographical data: $C_{32}H_{26}Cu_2N_{10}O_{13}$, Fw = 885.71, Monoclinic, *C*2/*c*, *a* = 28.84(4), b = 7.642(10), *c* = 18.79(2) Å, *V* = 3559(8) $Å^3$, *Z* = 4, D_c = 1.653 g/cm^3, R_1 = 0.0452, wR_2 = 0.1615, GOF = 1.116.

Table S1. The element distribution of CuBMMB.

			Content of N 1s groups (%)			Content of O 1s groups (%)			
Element	Apparent Concentration	wt%	Pyridinic-N	Pyrrolic-N	Cu-N	H-O	Cu-O (Cu-O)	N-O	C-O
C	142.54	73.25	-	-	-	-	-	-	-
O	5.70	4.43	-	-	-	11.09	38.87	40.98	9.06
N	18.45	15.05	51.9	30.45	17.65	-	-	-	-
Cu	9.71	7.27	-	-	-	-	-	-	-
Total		100	-	-	-	-	-	-	-

Table S2. The value of total nitrogen element at different times.

Time (h)	Concentration (NO_3^--N+NH_4^+-N+NO_2^-) (ppm)
0	200
1	202.75
2	204
3	208
4	208.4
5	208.7

Table S3. The value of ion chromatography and colorimetric methods for the concentration of produced nitrite and ammonium as well as residual nitrate.

	Colorimetric methods (dilution times)	Ion chromatography (dilution times)
Ammonium	**146.4 (250)**	**147.3 (3000)**
Nitrite	**8.3 (50)**	**9 (10)**
Nitrate	**54 (100)**	**51.6 (200)**
Total	**208.7**	**207.9**

Table S4. Performance comparison.

Cathode material	Cathode Area (cm2)	Electrolytes	NO_3^- conversion (%)	Selectivity (%)	Reaction time (h)	Article
Pd/Zr-MOF	1	500 ppm $NaNO_3$+0.1 M Na_2SO_4	-	- (NH_4^+)	0.5	[24]
Ru_xO_y/RuNi-MOF	4	50 ppm $NaNO_3$+0.1 M Na_2SO_4	-	100 (NH_4^+)	1	[25]
Cu/Th-MOF	1	100 mM $NaNO_3$+1 M KOH	-	-(NH_4^+)	2	[34]
CuBMMB (This work)	1	200 ppm KNO_3+1 M KOH	73.3	96.5 (NH_4^+)	5	This work
Cu/CuHHTP	1	500 ppm $NaNO_3$+0.5 M Na_2SO_4	85.81	97 (NH_4^+)	2	[35]
Cu/Ce-MOF	1	5 mM $NaNO_3$+0.5 M Na_2SO_4	80.6	100 (NH_4^+)	4	[40]

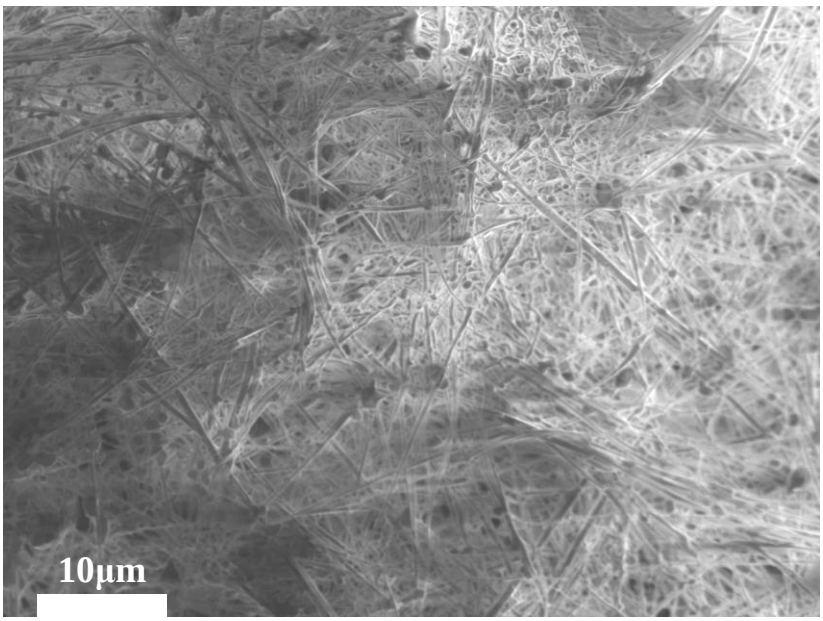

Figure S1. SEM image of the CuBMMB.

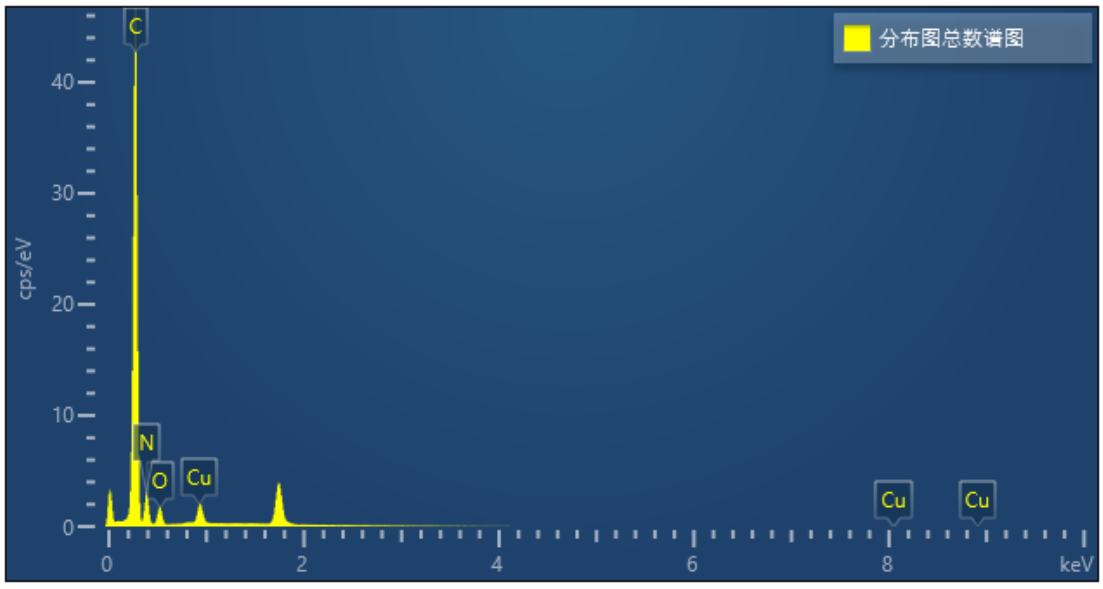

Figure S2. The EDS images of the CuBMMB.

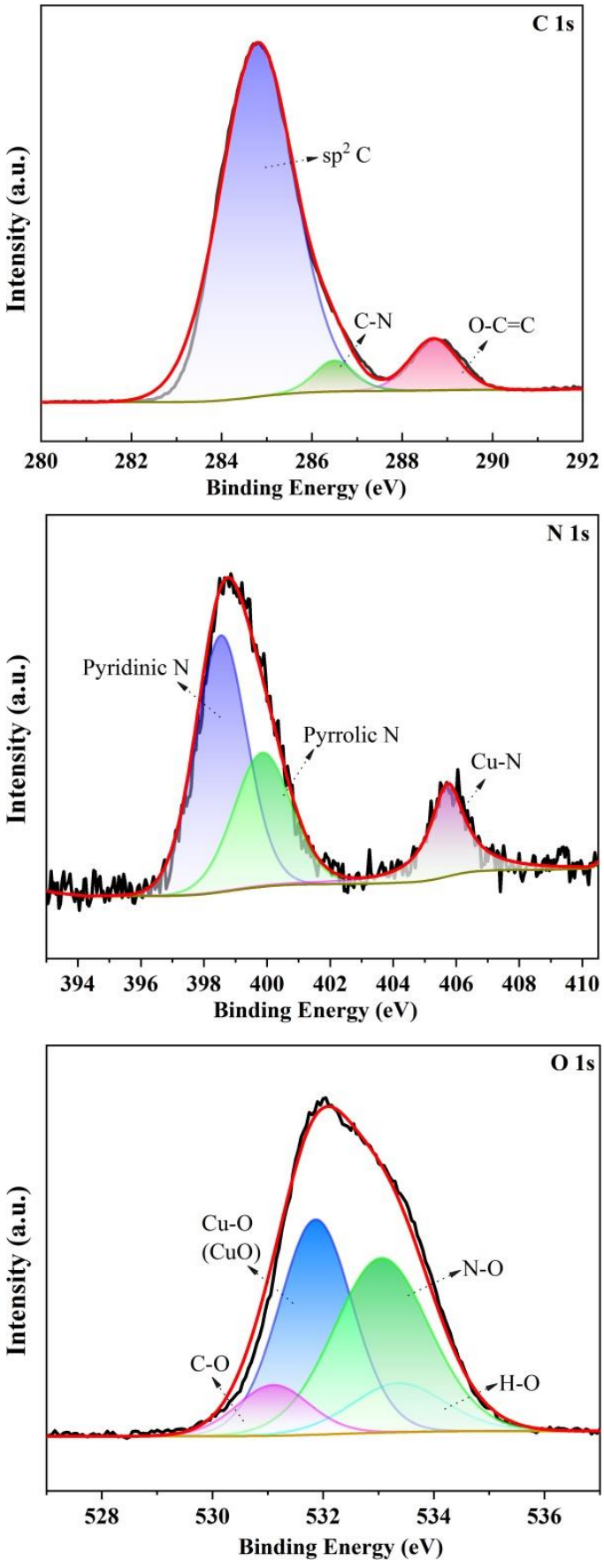

Figure S3. The XPS survey of C 1s, N 1s, and O 1s.

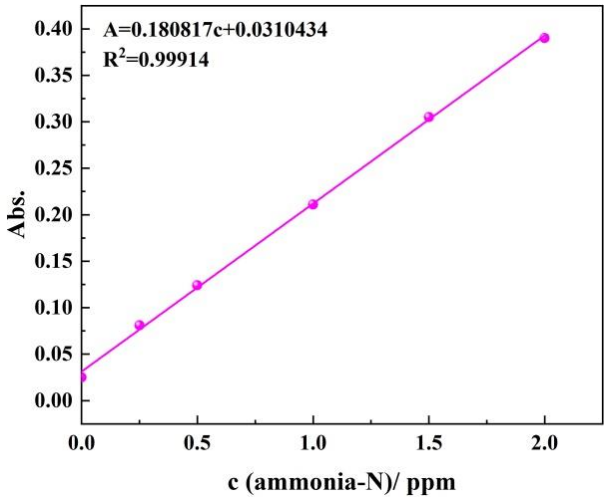

(a)

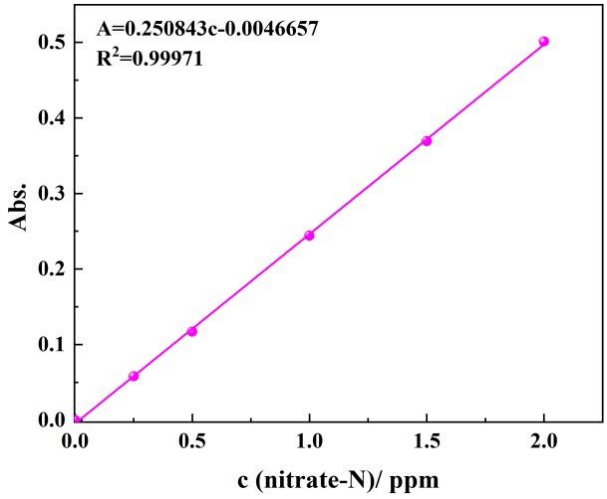

(b)

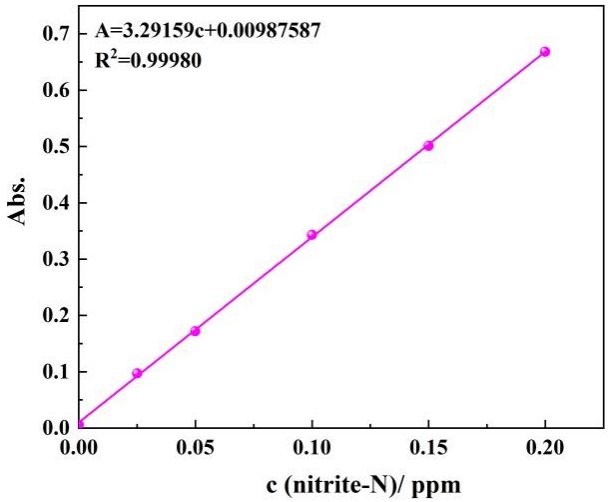

(c)

Figure S4. Concentration-absorbance calibration curves of (a) ammonia-N, (b) nitrate-N, and (c) nitrite-N.

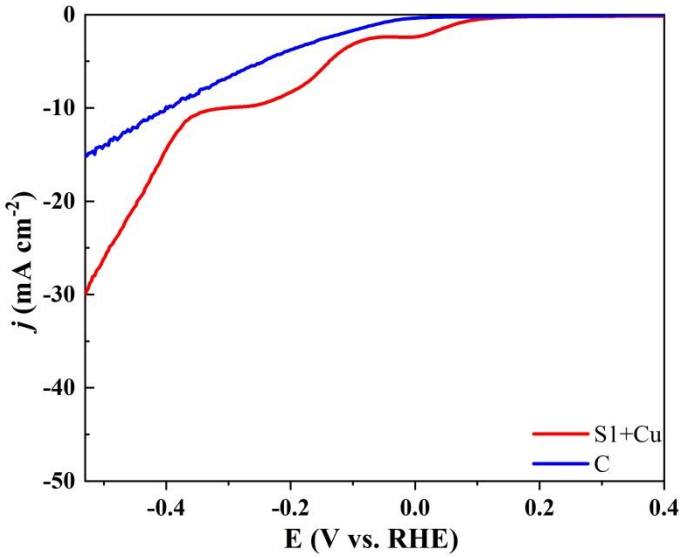

Figure S5. LSV curves in 1 M KOH electrolyte with 200 ppm NO_3^--N.

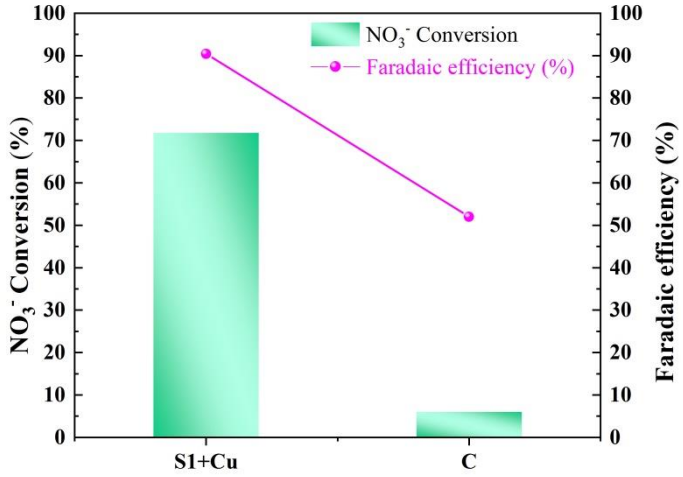

Figure S6. Faradaic efficiency and nitrate conversion of the CuBMMB and carbon cloth in 1 M KOH electrolyte with 200 ppm NO_3^--N at −0.53 V (vs. RHE).

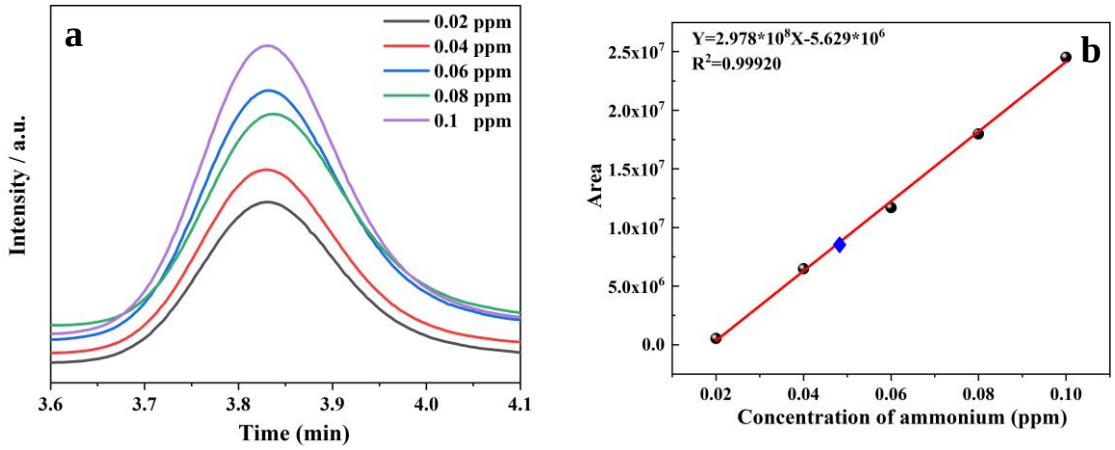

Figure S7. (a) Ion chromatogram (IC) curves of the time-dependent ammonium production for a series of standard ammonium solutions and CuBMMB at −0.53 V; (b) calibration curve of IC for ammonium concentration.

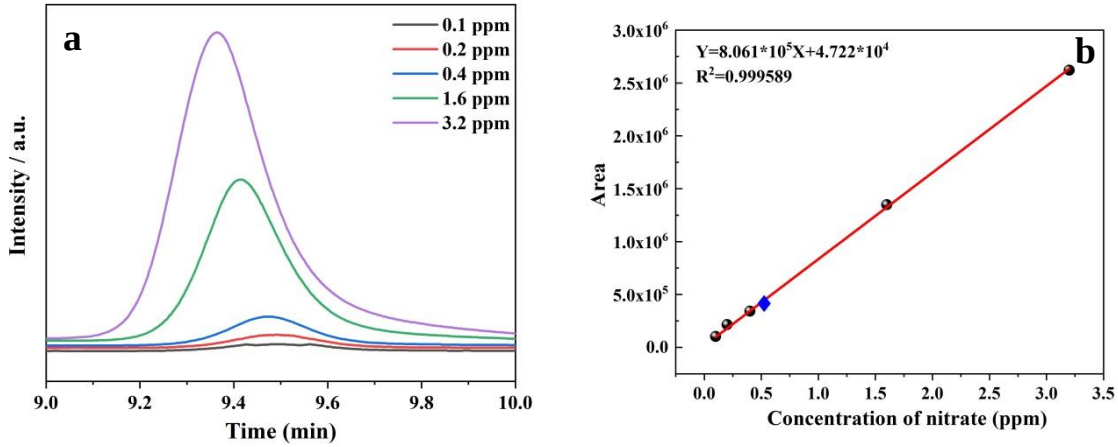

Figure S8. (a) IC curves of the time-dependent nitrate residue for a series of standard nitrate solutions and CuBMMB at −0.53 V; (b) calibration curve of IC for nitrate concentration.

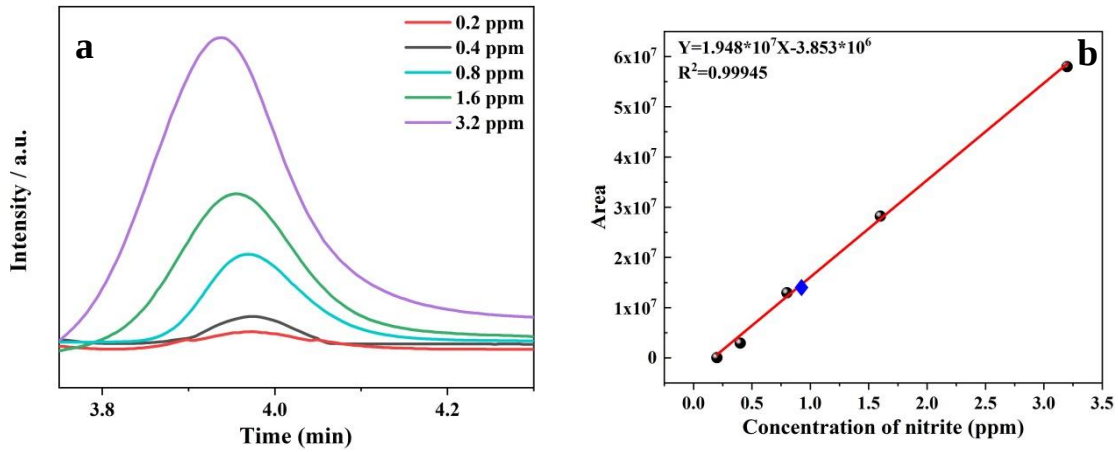

Figure S9. (a) IC curves of the time-dependent nitrite production for a series of standard nitrite solutions and CuBMMB at −0.53 V; (b) calibration curve of IC for nitrite concentration.

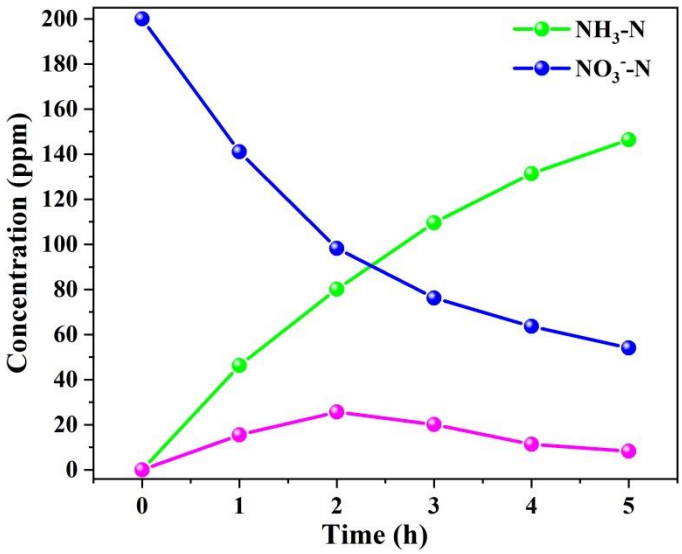

Figure S10. Time-dependent concentration of NO_3^-, NO_2^-, and NH_4^+ over CuBMMB at −0.53 V vs. RHE.

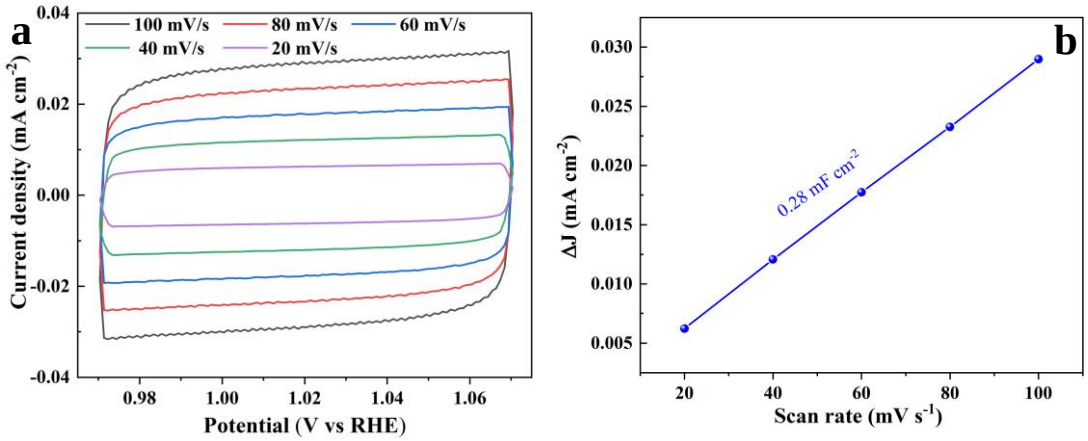

Figure S11. (a) CV curves of the CuBMMB at different scanning rates (10–100 mV s^{-1}); (b) relationship between the scanning rate and the current density of Cu-MOF.

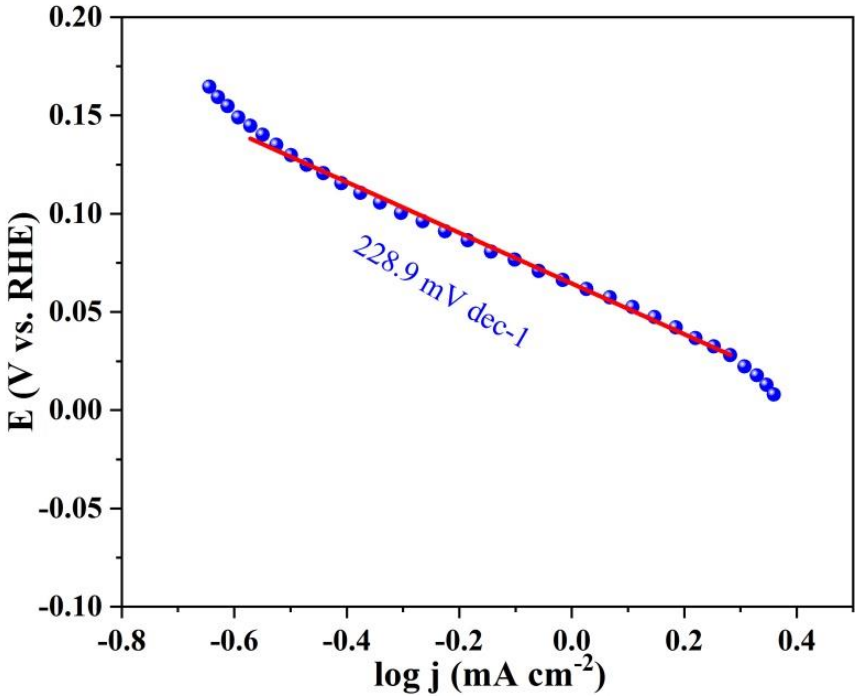

Figure S12. Tafel plot of CuBMMB in 1 M KOH electrolyte with 200 ppm NO_3^--N.

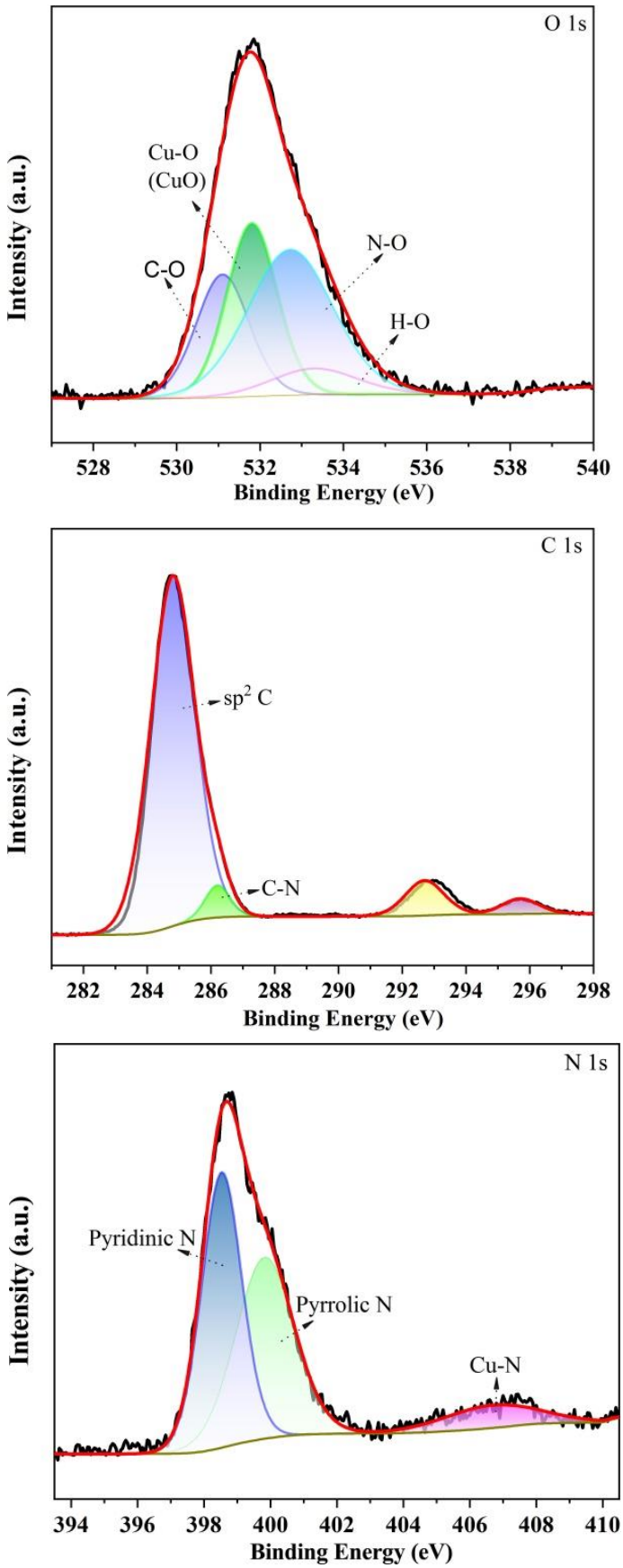

Figure S13. The XPS survey of C 1s, N 1s, and O 1s after NRA.

Reference

[3] Eaton, A. D.; Clesceri, L. S.; Greenberg, A. E.; Franson, M. A. H., Standard methods for the examination of water and wastewater. Am J Public Health Nations Health 1966, 56 (3), 387-388.

[5] Wang, Y.; Yu, Y.; Jia, R.; Zhang, C.; Zhang, B., Electrochemical Synthesis of Nitric Acid from Air and Ammonia through Waste Utilization. Natl. Sci. Rev. 2019, 6, 730.

[24] JIANG M, SU J, SONG X, et al. Interfacial Reduction Nucleation of Noble Metal Nanodots on Redox-Active Metal–Organic Frameworks for High-Efficiency Electrocatalytic Conversion of Nitrate to Ammonia [J]. Nano Letters, 2022, 22(6): 2529-37.

[25] QIN J, WU K, CHEN L, et al. Achieving high selectivity for nitrate electrochemical reduction to ammonia over MOF-supported RuxOy clusters [J]. Journal of Materials Chemistry A, 2022, 10(8): 3963-9.

[29] WANG Y, XU A, WANG Z, et al. Enhanced Nitrate-to-Ammonia Activity on Copper–Nickel Alloys via Tuning of Intermediate Adsorption [J]. Journal of the American Chemical Society, 2020, 142(12): 5702-8.

[30] LI J, GAO J, FENG T, et al. Effect of supporting matrixes on performance of copper catalysts in electrochemical nitrate reduction to ammonia [J]. Journal of Power Sources, 2021, 511(

[34] GAO Z, LAI Y, TAO Y, et al. Constructing Well-Defined and Robust Th-MOF-Supported Single-Site Copper for Production and Storage of Ammonia from Electroreduction of Nitrate [J]. ACS Central Science, 2021, 7(6): 1066-72.

[35] ZHU X, HUANG H, ZHANG H, et al. Filling Mesopores of Conductive Metal–Organic Frameworks with Cu Clusters for Selective Nitrate Reduction to Ammonia [J]. ACS Applied Materials & Interfaces, 2022, 14(28): 32176-82.

[36] XU Y-T, XIE M-Y, ZHONG H, et al. In Situ Clustering of Single-Atom Copper Precatalysts in a Metal-Organic Framework for Efficient Electrocatalytic Nitrate-to-Ammonia Reduction [J]. ACS Catalysis, 2022, 12(14): 8698-706.